Analysis of the high-speed rotary motion of a superconducting magnetic bearing during ring spinning

Engineering Research Express

PAPER

Analysis of the high-speed rotary motion of a superconducting magnetic bearing during ring spinning

Maria Sparing[1], **Tilo Espenhahn**[1], **Günter Fuchs**[1], **Mahmud Hossain**[2], **Anwar Abdkader**[2], **Kornelius Nielsch**[1], **Chokri Cherif**[2] **and Ruben Hühne**[1]

[1] Leibniz IFW Dresden, Institute for Metallic Materials, Helmholtzstrasse 20, 01069 Dresden, Germany
[2] Faculty of Mechanical Engineering, Technische Universität Dresden, Institute of Textile Machinery and High Performance Material Technology (ITM), Hohe Strasse 6, 01069 Dresden, Germany

E-mail: r.huehne@ifw-dresden.de

Keywords: superconducting magnetic bearing, high speed rotation, 3D ring motion, dynamic properties

OPEN ACCESS

RECEIVED
19 June 2020

REVISED
1 September 2020

ACCEPTED FOR PUBLICATION
11 September 2020

PUBLISHED
22 September 2020

Abstract

Ring spinning is the leading textile technology for the production of short staple yarn, which runs commercially up to a maximum speed of 25 000 rpm. Higher speeds result in yarn damage mainly due to frictional heat. To eliminate this limitation, a friction-free superconducting magnetic bearing (SMB) was introduced as alternative high-speed yarn twist element consisting of a cryostat with an array of superconductors and a levitating permanent magnet ring with a yarn guide. Whereas stable spinning was possible until 30 000 rpm, it turned out that the new SMB twist element is more susceptible to external disturbances resulting in oscillating movements of the magnet. Therefore, a measurement system with an array of 5 synchronized optical laser triangulation sensors and one tachometer was implemented to analyse this motion in detail during spinning with high speeds. To test the system, the spinning speed was varied between 10 000 rpm and 21 000 rpm for different yarn qualities. In general, the magnetic ring oscillates around its centre position with the rotation frequency and a peak amplitude between 10 μm and 14 μm, which might be due to a small imbalance of the magnet. At the same time, the small tilt of the ring remained fixed with respect to the machine for all speeds. In addition, larger oscillation amplitudes of up to 300 μm are observed at 18 Hz for selected spinning parameters arising most probably from resonance effects with machine vibrations.

1. Introduction

Superconducting magnetic bearings (SMB) are passive self-stabilized devices, which usually consist of a superconductor cooled below its critical temperature in the presence of a permanent magnet [1, 2]. SMBs were studied for a number of applications, where the transport of high loads [3–5] and/or fast rotary movements without contact friction are desired [6–9]. Recent activities of our group are focused on the application of such SMBs in state-of-the-art textile machines to improve their performance significantly. In particular, ring spinning is a leading technology for the production of short staple yarn in textile industry [10, 11]. In this technology, a fibrous material (e.g. cotton, polyester) is twisted into yarn by a so-called ring-traveler twist element, i.e. by a small metal clip ('traveler') moving on a ring-shaped body. However, this commercial ring spinning technology is limited to a maximum speed of about 25 000 rpm as the frictional heat between ring and traveler leads to yarn damage for higher speeds like the fusion of thermoplastic fibres.

We recently showed that the application of a SMB twist element in the ring spinning process allows to eliminate the productivity limiting contact friction of the conventional ring-traveler twist element [12, 13]. In this case, the twist is imparted by a levitating NdFeB permanent magnet (PM) ring, which is driven by the yarn winding onto the bobbin (spindle) as illustrated in figure 1 and described in more detail in previous publications [14, 15]. Compared to the conventional ring-traveler twist element, considerably higher spinning speeds might be achieved with such a SMB based setup due to the significantly reduced contact friction. In general, our test

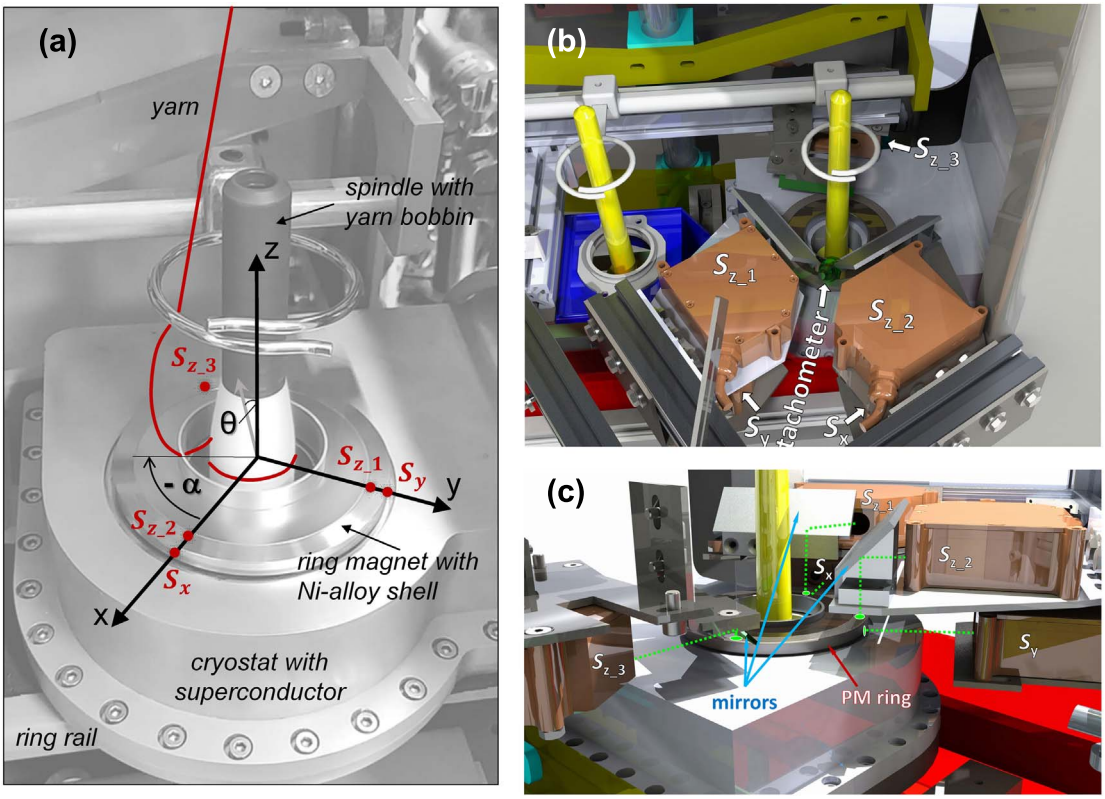

Figure 1. Ring spinning with a SMB twist element: (a) The fibrous material is continuously delivered by a set of delivery rollers above the spindle (not shown). The rotating spindle winds the yarn onto the bobbin and thereby drives the freely levitating ring magnet and imparts twist in the yarn. The coordinate system illustrates the position of the measurement points of the optical laser sensor array on the surface of the ring magnet; Schematic top (b) and side (c) view of the SMB with the installed sensor array; *S* denote the different sensors, the optical beams a sketched with green lines.

setup is designed for a speed of up to 50 000 rpm. With the prospect to increase the productivity of the ring spinning process by more than a factor of two, the SMB twist element is also beneficial from the economic point of view.

So far, a stable spinning process was achieved for a speed of 30 000 rpm with the new setup [16]. It turned out during these studies that the new SMB is susceptible to process-related machine vibrations resulting in oscillating movements of the rotating PM, which in turn influences the yarn quality and might even result in yarn breakage. To characterize the behaviour of the SMB in this complex process and to identify possible solutions for an improved stability, it is necessary to measure and analyse the high-speed motion of the rotating PM ring itself. It should be noted at this place that the interaction between the rotating PM and the yarn is not yet completely understood and deserves a detailed study. Up to now, the SMB is described as a simple spring-mass-damper system, in which the PM is driven by an external point force (i.e. the yarn) [13, 17]; however, no measurement data was available so far to validate this model in detail.

Most rotational SMBs developed in the past have an axial configuration, i.e. concentric PM and superconductor rings. They are mainly used for flywheel energy storage systems with a rotational speed of up to 30 000 rpm [2, 6, 7, 18, 19]. Alternatively, parallel setups were studied for this purpose [20, 21]. These SMBs are usually characterized by measuring magnetic forces in dependence of the displacement in order to determine their stiffness. Additionally, the damping of external disturbances is measured. For some systems, dynamic measurements on a SMB at high speeds were performed on the rotor of the device [22, 23].

In the following, we will present a new experimental setup, which allows to track the high-speed motion of the freely rotating PM ring *in situ* during the ring spinning process. The analysis of the PM ring motion (time-dependent position and tilt with regard to the cryostat) during the real process is a first step on the way to understand, how the individual spinning parameters influence the spinning process with an SMB twist element. The long-term objective of our work is to establish an all-encompassing model of the interaction between the dynamic yarn motion and SMB twist element in the non-stationary ring spinning process in order to optimize the technology for speeds above 30 000 rpm.

2. Set up of the SMB and the measurements

2.1. Setup of SMB twist element

The core component of the SMB twist element is a segmented ring of a $YBa_2Cu_3O_{7-x}$ (YBCO) bulk superconductor inside a liquid nitrogen bath cryostat, which is cooled to 66 K by reducing the gas pressure in the cryostat to 125 mbar [16]. Above the cryostat an axially magnetized NdFeB ring (inner diameter: 50 mm, outer diameter: 80 mm, height h: 6 mm, mass: ~270 g) with an eyelet insert for the yarn is field-cooled parallel to the superconductor ring at a distance of 3 mm (i.e. 1 mm above the upper cryostat wall). The magnetic flux density distribution of this setup was studied in detail in a previous publication [24]. The PM ring is reinforced by a 7 mm shrunk fit Nickel-alloy shell to withstand the calculated centrifugal forces at a rotational speed of 50 000 rpm using simulations as described previously [13]. The SMB twist element is placed on top of the ring rail inside the ring spinning machine (see figure 1).

The resonance frequencies f and decay constants δ of the SMB twist element at 66 K were measured with a 3-axis piezoelectric acceleration sensor (Typ 4506-B, *Brüel & Kjær*) using a set up described previously [13] to be approximately $f_{rad} = 15$ Hz, $f_{ax} = 30$ Hz, $\delta_{rad} = 5\ s^{-1}$ and $\delta_{ax} = 10\ s^{-1}$, respectively, for the SMB setup used in the following experiments. The resulting dynamic radial bearing stiffness constant k is 2.5 N mm^{-1}. The yarn tension between the eyelet connected to the magnet and the spindle, which is a measure for the pulling force at the magnet, increases almost linear from about 50 cN at 15 000 rpm to 175 cN at 30 000 rpm [16].

2.2. Setup of optical distance sensor array

The displacement of the PM ring is recorded during the spinning process by a set of 5 synchronized optical laser triangulation sensors (optoNCDT 2300 series by *Micro-Epsilon*), which are mounted with a rigid frame directly onto the ring rail. They generate a signal linear to the distance between sensor and PM with a resolution of 300 nm and a measuring rate of 20 kHz. Two of the displacement sensors, S_x and S_y, are placed laterally of the magnetic ring with a 90° angle to each other defining the x-y measurement plane E_0. The three other sensors are positioned above the magnetic ring at fixed x-y coordinates with a 90° angle between sensor S_{z_1} and S_{z_2} and 135° to sensor S_{z_3}, as illustrated in figure 1. In this case, a 90° mirror is used to measure the distance in z-direction (i.e. perpendicular to E_0). In addition, a brightness sensor is used as tachometer tracing the speed of the rotating ring having a bright-coloured section. It is placed between the two lateral sensors S_x and S_y. From the measured changes in distance over time, the motion (tilt and displacement in x, y and z direction) of the magnet ring's geometric centre $x_{MP}(t)$, $y_{MP}(t)$, $z_{MP}(t)$ is calculated using geometric and function solvers in the programming language Python.

2.3. Calculation of the PM ring centre from measurement data

The origin of a Cartesian coordinate system fixed with respect to the cryostat and the optical sensors is defined by the x-y measurement plane E_0 and the geometric centre of the field-cooled PM ring. The initial position of the top PM surface is denoted as plane E_z with $z = h/2$, which is parallel to the x-y measurement plane E_0 after field-cooling.

The tilt $\theta(t)$ of the PM during spinning is calculated from the angle between the plane $E_z(t)$ defined by the measurement points $z_1(t)$, $z_2(t)$ and $z_3(t)$ (with known x_i, y_i for each sensor) and the initial top surface E_z (or the parallel plane E_0).

The two lateral measurement points S_x $(0, y(t), 0)$ and S_y $(x(t), 0, 0)$ at the outer ring surface define two points of an ellipse, which arises from the intersection of the measurement plane E_0 with the cylindrical surface of the PM ring tilted by an angle θ (figure 2). In other words, we describe a cylindric section, where the resulting ellipse is situated in the measurement plane E_0 and the cylinder (i.e. the magnet ring with height h) is tilted by an angle θ as well as is shifted in x, y and z direction. The centre of this rotated ellipse (x_m, y_m) can be calculated solving equation (1) for the measurement points S_x and S_y.

$$\frac{[(x - x_m)\cos\alpha + (y - y_m)\sin\alpha]^2}{a^2} + \frac{[(x - x_m)\sin\alpha - (y - y_m)\cos\alpha]^2}{b^2} = 1 \quad (1)$$

The length of the semi-major half axis $a(t)$ is:

$$a = \frac{R}{\cos\theta} \quad (2)$$

with R being the radius of the magnet ring and equally the length of the semi-minor half axis b.

The rotation angle $\alpha(t)$ of this ellipse with respect to the coordinate system is defined as the smallest angle between the positive x-axis and the orientation of the semi-major half axis a. If the magnetic ring is not displaced in z-direction (i.e. $z_{MP}(t) = 0$), the calculated coordinates x_m and y_m from equation (1) are equivalent to $x_{MP}(t)$, $y_{MP}(t)$. Otherwise, the centre of the PM ring is calculated as follows: the top base plane $E_z(t)$ is shifted along its

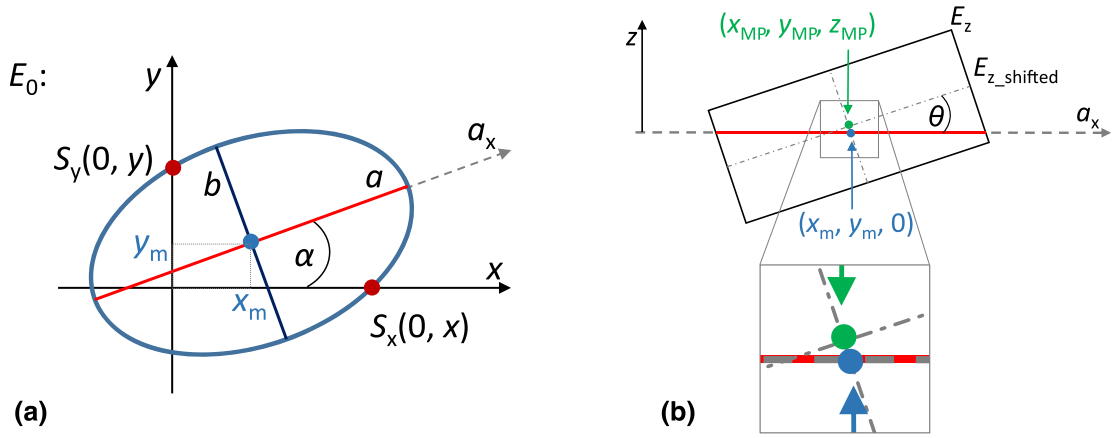

Figure 2. (a) Ellipse from the tilted PM ring in the E_0 (x-y-0) plane (the ellipticity is strongly enhanced compared to reality). (b) View of the tilted PM ring (cylinder) cutting through the E_0 plane. The cut is shown along the half-major axis of the ellipse, i.e. at the maximum tilt angle θ with the x-axis being rotated by α (not to scale).

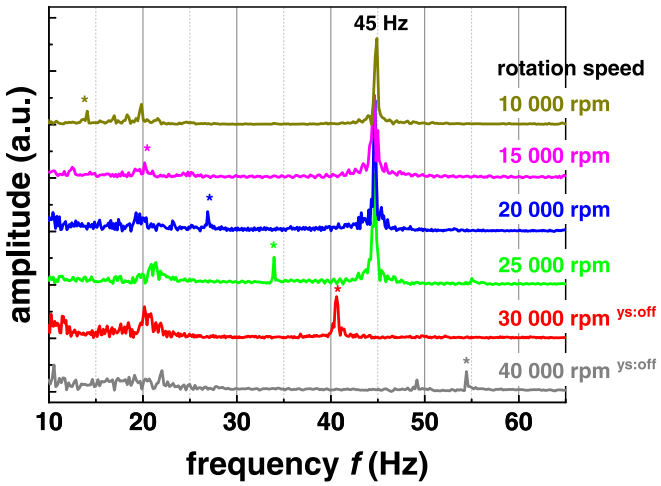

Figure 3. Vibrations recorded on the ring rail itself during the downwards movement at different spinning speeds. The peaks marked with an asterisk * shift with the rotation speed and are correlated to the gear transmission ratio of the spindle drive. The 45 Hz peaks originate from the yarn suction motor (ys) which was switched off at 30 000 rpm and 40 000 rpm for this measurement.

normal towards E_0 by $h/2$ (dashed-dotted line in figure 2(b)). The centre of the magnetic ring is always in this plane $E_{z\_shifted}(t)$. Subsequently, $x_{MP}(t)$, $y_{MP}(t)$, and $z_{MP}(t)$ are derived by an orthogonal projection of the centre of the ellipse (x_m, y_m, 0) into the plane $E_{z\_shifted}(t)$ (blue and green point in figure 2(b)).

3. Results and discussion

3.1. Influence of machine vibrations on the SMB without rotation of the PM

The cryostat with the SMB twist element is rigidly mounted onto the ring rail of the ring spinning machine. This ring rail moves up and down with respect to the rotating spindle during the spinning process to allow for an even distribution of the yarn onto the bobbin. The optical sensor array is also mounted on the ring rail with an additional framework. Consequently, vibrations of the ring rail will affect both the sensor array and the PM ring in the SMB, respectively. Therefore, we studied these vibrations using 3-axis acceleration sensors on the ring rail and the SMB, respectively.

Figure 3 gives an example of the vibrations recorded on the ring rail itself during the downwards movement at different spinning speeds. The peaks marked with an asterisk * shift with the rotation speed and are correlated to the gear transmission ratio of the spindle drive. The 45 Hz peak originates from the operating frequency of a yarn suction (ys) motor, which propagates into the ring rail and further into the sensor mounting and the SMB. For comparison, this yarn suction was switched off above 25 000 rpm leading to the extinction of the related peak in the frequency spectra. However, the yarn suction is a necessary feature for ring spinning of yarn and

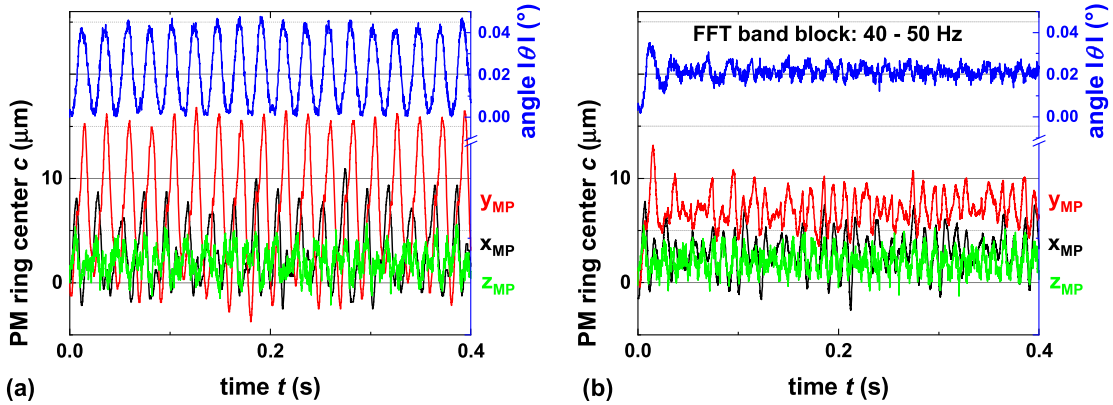

Figure 4. Calculated values for PM ring centre position and tilt θ determined from measurements on a fixed magnet within a running machine (a) without and (b) with 40–50 Hz band block to qualify the influence of the machine vibration on the sensor signal.

cannot be omitted. Below 25 Hz are a number of low frequency vibrations of unknown origin, arising most probably from different moving parts in the ring spinning machine itself. Unfortunately, it is not possible to avoid these low frequency machine vibrations completely; therefore, they need to be considered during data analysis.

In a next step, the influence of machine vibrations on the optical sensor array, which is directly mounted on the ring rail, is evaluated. Therefore, the position of the non-rotating PM ring is recorded with this sensor array for a fixed field-cooling position (i.e. no freely levitating PM), but with running spinning machine (though no spinning) and yarn suction. Figure 4(a) shows the analysed coordinates of the PM ring centre as well as the absolute value of the tilt angle θ. Most notably are the oscillation of the signals with a frequency of 45 Hz. They can be correlated to the operating frequency of the yarn suction motor, which propagates into the ring rail and thereby also into the sensor mounting. An FFT band block of this frequency reduces the noise in the calculated data to a level of about $+/-3$ μm or 0.005° (figure 4(b)). The accuracy of the measurement may be improved in the future by a further stiffening of the frame for the sensor array.

3.2. Motion of the magnetic ring during spinning

The motion of the PM ring in the SMB was studied during spinning at various spindle speeds between 10 000 rpm and 21 000 rpm with three different cotton yarn qualities of 20 tex, 30 tex and 40 tex yarn count, respectively (1 tex $=$ 1 g per 1000 m yarn). The data were always taken during the uniform movement of the ring rail (i.e. not at the reversal points), so that an almost constant yarn force is acting on the magnet. As an example, the calculated coordinates of the PM ring centre as well as the angles θ and α are shown in figure 5 for a speed of 19 000 rpm and a yarn count of 20 tex.

The vertical lines represent the tachometer signal, i.e. the start of the bright marker on the PM. The distance indicates one full rotation of the yarn and the PM ring around the spindle. The FFT (not shown) of the tachometer signal reveals a mean rotation frequency of the PM at 310 Hz (18 600 rpm), which is 2.1% less than the nominal driving speed of the spindle of 316 Hz. The speed difference between magnet and spindle, which is in the same range as the speed difference between traveler and spindle in classical ring spinning, is an important prerequisite for the winding of the yarn on the bobbin. For the SMB twist element this difference most likely originates from the air friction of the yarn balloon and the friction between the yarn and the eyelet fixed on top of the PM ring.

As shown in figure 5(a), the coordinates of the PM ring centre $x_{MP}(t)$ and $y_{MP}(t)$ change periodically. The movement can be described by a superposition of an oscillation with a small peak amplitude of about $+/-14$ μm at a frequency of 310 Hz and one with a larger amplitude of about $+/-200$ μm at 18 Hz frequency, respectively. In z-direction, the amplitude is much smaller for the 310 Hz oscillation with maximum values of about $+/-5$ μm and less prominent at 18 Hz.

The tilt angle $\theta(t)$ and the rotation angle $\alpha(t)$ of the ellipse are shown in figure 5(b). The mean absolute tilt angle $\theta(t) = -0.82°$ oscillates slightly ($\sigma = 0.02°$) with the rotation frequency of 310 Hz. It remains on a nearly constant value for all investigated yarn counts and speeds above 15 000 rpm. The mean rotation angle of the tilted ellipse $\alpha(t)$ shows a similar behaviour. It oscillates with 310 Hz around a mean of $= -86.4°$ ($\sigma = 1.1°$) as well. The fact, that α only varies between $-83°$ and $-89°$ indicates, that the tilt $\theta(t)$ of the PM does not rotate around the central SMB axis, while the PM itself rotates with 310 Hz around its axis. In other words, while the PM rotates, the slight tilt $\theta(t)$ is almost fixed with respect to the sensors and the whole machine. This behaviour

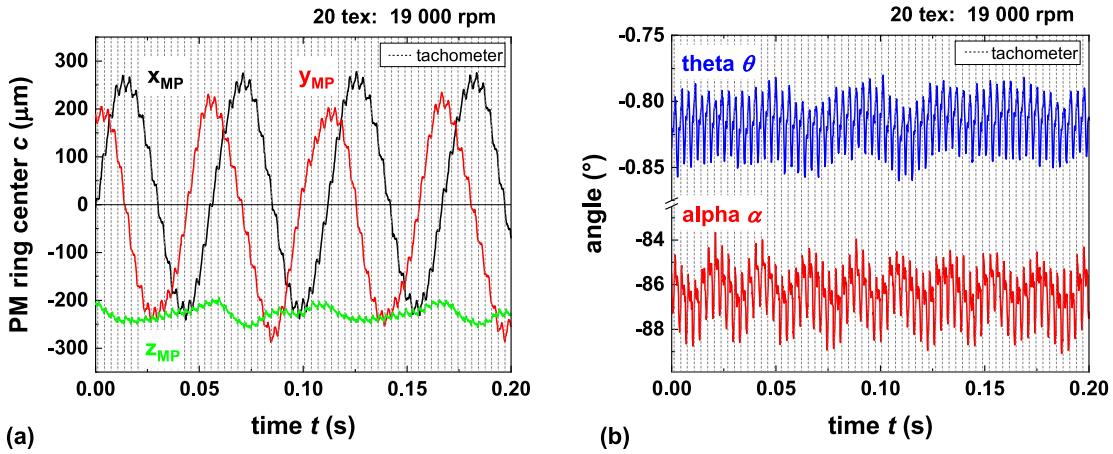

Figure 5. (a) Calculated coordinates of the PM ring centre and (b) angles θ and α for 20 tex yarn at 19 000 rpm. The vertical lines represent the tachometer signal, each indicating one full rotation of the yarn and the PM ring around the spindle.

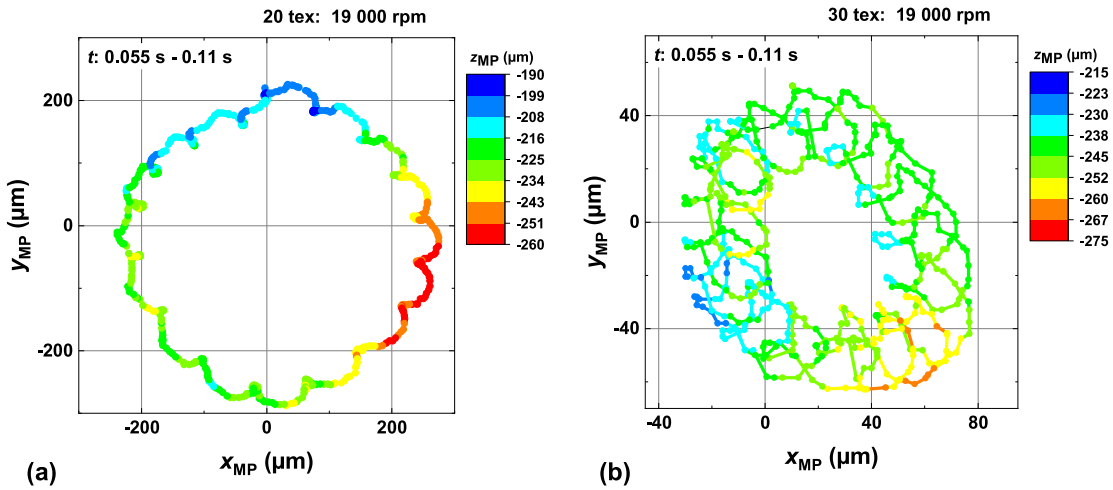

Figure 6. PM ring centre position $y_{MP}(t)$ over $x_{MP}(t)$ for a time interval of 0.055 s during spinning at 19 000 rpm for (a) 20 tex and (b) 30 tex yarn count. The color of the data points gives the height of the ring centre $z_{MP}(t)$.

was observed for all investigated yarn counts and speeds. Additional measurements (not shown) reveal that the value of α changes, when the field cooling position of the PM is modified. This suggests that the main contribution to the tilt θ originates from the non-uniformity of the bearing over the circumference and is not the result of a force exerted by the rotating yarn.

In figure 6, the PM ring centre is plotted as $y_{MP}(t)$ over $x_{MP}(t)$ for a time interval of 0.055 s during spinning at 19 000 rpm using a yarn count of 20 tex (figure 6(a), same dataset as in figure 5(a)) as well as for 30 tex (figure 6(b)), respectively. The colour of the data points indicates the height of the ring $z_{MP}(t)$. During this time interval, the PM ring centre moves one complete turn around its initial (i.e. non-spinning) centre for both yarn counts; however, the overall diameter of this circle is much smaller for 30 tex compared to 20 tex yarn (see also figure 8(a)). The centre of the PM ring rotates around the geometric (initial) centre with a frequency of approximately 18 Hz (1/0.055 s = 18.2 Hz) for all yarn counts above 15 000 rpm. This frequency is independent of the rotation speed as visible in the FFT plots of $y_{MP}(t)$ in figure 7 for 20 tex and 30 tex yarn count, respectively. Hence, the observed oscillation of the PM ring at 18 Hz cannot be attributed to a torque-induced precession, as the precession frequency ω_p would be inversely proportional to the rotation frequency ω_s.

In addition, the PM ring also rotates around its centre with the frequency of the spinning process. For example, the small arcs in figure 6(a) represent one rotation of the PM ring during spinning (17 small arcs in 0.055 s are equal to ~310 Hz).

To summarize the influence of spinning speed and yarn count on the peak amplitude of the oscillation $A(y_{MP})$ is plotted in figure 8 for all three yarn counts at (a) 18 Hz and (b) at the frequency of the rotation speed. For a yarn count of 20 tex the peak amplitude at 18 Hz increases beyond 100 μm for spinning speeds above

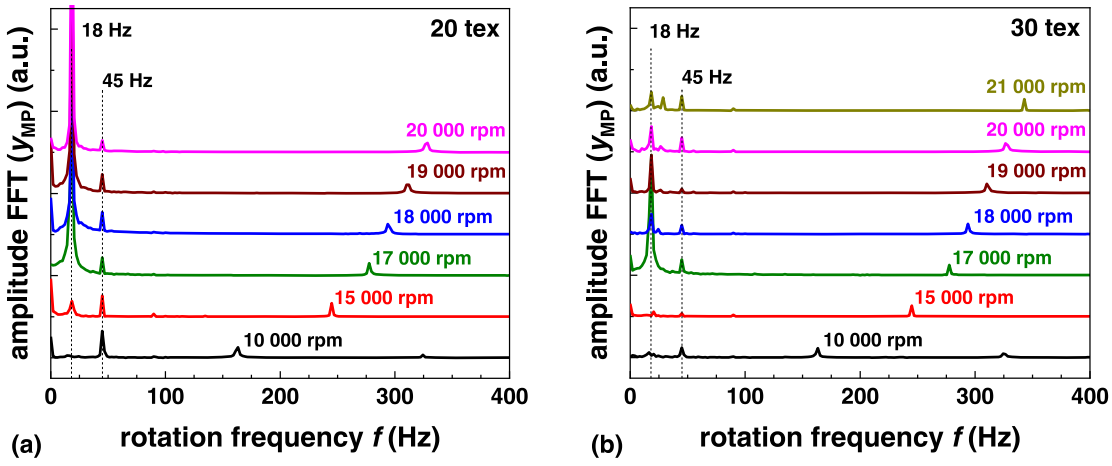

Figure 7. FFT plots of the PM ring centre position $y_{MP}(t)$ at various spinning speeds for: (a) 20 tex and (b) 30 tex yarn count.

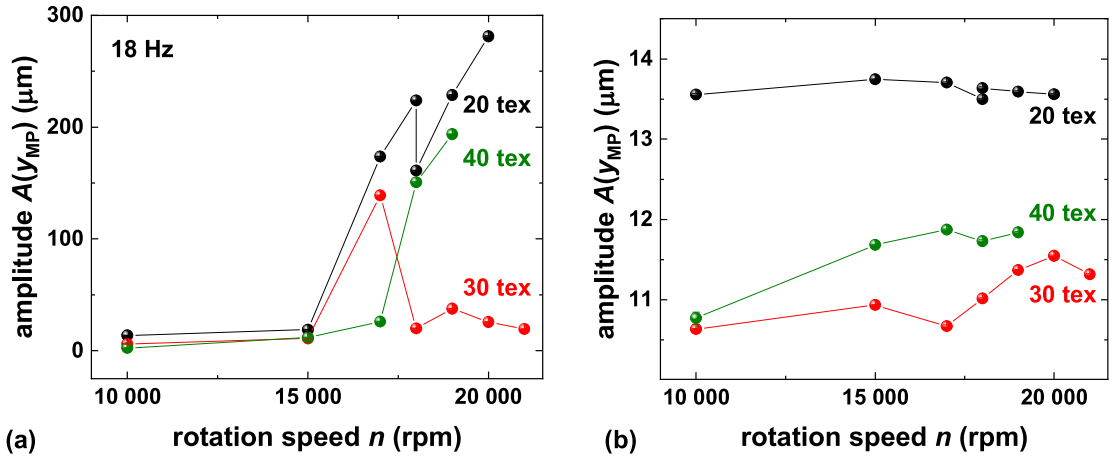

Figure 8. Peak amplitude of the oscillating PM ring centre position (y_{MP}) at 18 Hz (a) and at the frequency of the rotation speed (b).

15 000 rpm, i.e. the outer radius for the circular movement of the PM ring centre (see figure 6(a)) increases with spinning speed. At 18 000 rpm (20 tex) two data points are shown. Here the speed of the ring rail was reduced by increasing the needful yarn factor, i.e. the length of a complete layer or the quantity of yarn at each cycle of ring rail, from 7 to 10. This results in a reduction of the radius of displacement of the PM ring centre. Due to the complexity of the highly dynamic non-stationary spinning process, it is hitherto not understood if this is correlated to a reduction of the yarn force or other factors. The same holds for the measurement with a yarn count of 30 tex, where in contrast to 20 tex and 40 tex yarn the peak amplitudes at 18 Hz do not increase with the spinning speed and are comparatively smaller. The small peak amplitudes at the frequency of the rotation speed (figure 8(b)) are nearly constant at 13.5 μm for 20 tex yarn and between 11 and 12 μm for the 30 and 40 tex yarn with no clear trend for the yarn count or spinning speed.

The correlation of the measured amplitudes to external forces, e.g. the force exerted by the yarn onto the PM ring will be discussed elsewhere. The most likely scenario at this point is, that the observed 18 Hz oscillations at all spinning speeds are caused by resonance which is triggered by low frequency machine vibrations (figure 3). At a frequency close to the radial resonance frequency of 15 Hz a force below 0.3 N would be sufficient [17] for the observed peak amplitudes in figure 8(a).

The superimposed oscillations at the frequency corresponding to the rotation speed are not related to resonance. At the operation frequency of the spinning process (above 10 000 rpm), i.e. fare away from the resonance frequency of the bearing, the forces needed for a 10–15 μm lateral displacement of the PM ring by resonance alone would be higher than 4 N, which exceeds the tensile strength of the yarn. Instead, these small oscillations are most probably caused by unbalance of the magnet. The mass of the PM ring is unbalanced for the yarn eyelet, the yarn mass itself and the centrifugal forces acting on the yarn balloon. For example, the observed oscillation with a 14 μm peak amplitude might originate from an unbalanced mass of around 0.15 g. A detailed

analysis of such an unbalance will be the subject of further investigation with the aim to understand the interaction between yarn and SMB and, if possible, to deduce the yarn force at the eyelet from the displacement measurement.

4. Summary

The motion of the rotating magnetic ring in a SMB was successfully measured during ring spinning with an array of 5 synchronized optical laser triangulation sensors. The spinning speed was varied between 10 000 rpm and 21 000 rpm for three different yarn qualities. For all investigated parameters, the magnetic ring oscillates around its center position with the rotation frequency at a peak amplitude between 10 μm and 14 μm. This effect is most probably due to an unbalance caused by the eyelet or the yarn. In addition, larger oscillation amplitudes are observed at 18 Hz depending on the spinning parameters, which may originate from resonance triggered by low frequency machine vibrations. Due to the complexity of the highly dynamic non-stationary spinning process, it is not yet fully understood how the observed oscillations are correlated to the spinning parameters and the force exerted by the yarn onto the PM ring. Nevertheless, we could show that the new measurement setup enables a deeper inside in the high-speed ring spinning process with a SMB twist element.

Acknowledgments

This work was supported by the German Research Foundation, DFG through project CH 174/33-2 and SCHU 1118/12-2.

ORCID iDs

Maria Sparing https://orcid.org/0000-0003-1653-048X
Tilo Espenhahn https://orcid.org/0000-0002-7621-8810
Ruben Hühne https://orcid.org/0000-0002-0030-6048

References

[1] Hull J R 2000 Superconducting bearings *Supercond. Sci. Technol.* **13** R1
[2] Ma K B *et al* 2003 Superconductor and magnet levitation devices *Rev. Sci. Inst.* **74** 4989–5017
[3] Deng Z *et al* 2017 A high-temperature superconducting maglev-evacuated tube transport (HTS Maglev-ETT) test system *IEEE Trans. Appl. Supercond.* **27** 3602008
[4] Schultz L *et al* 2005 Superconductively levitated transport system—the SupraTrans project *IEEE Trans. Appl. Supercond.* **15** 2301–5
[5] Sotelo G G *et al* 2014 MagLev Cobra: test facilities and operational experiments *J. Phys. Conf. Ser.* **507** 032017
[6] Werfel F N *et al* 2012 Superconductor bearings, flywheels and transportation *Supercond. Sci. Technol.* **25** 014007
[7] Strasik M *et al* 2010 An overview of Boeing flywheel energy storage systems with high-temperature superconducting bearings *Supercond. Sci. Technol.* **23** 034021
[8] Klöppel S *et al* 2017 Superconducting bearings for a LHe transfer pump *IOP Conf. Ser.: Mater. Sci. Eng.* **278** 012029
[9] Koshizuka N 2006 R&D of superconducting bearing technologies for flywheel energy storage systems *Physica* C **445–448** 1103–8
[10] Gries T and Veit D 2015 *Textile Technology: An Introduction* (Munich: Carl Hanser Verlag)
[11] Klein W 1998 *The Technology of Short-Staple Spinning* (Manchester: The Textile Institute)
[12] Hossain M *et al* 2014 Innovative twisting mechanism based on superconducting technology in a ring-spinning system *Text. Res. J.* **84** 871–80
[13] Sparing M *et al* 2015 Superconducting magnetic bearing as twist element in textile machines *IEEE Trans. Appl. Supercond.* **25** 3600504
[14] Berger A *et al* 2016 Cryogenic system for the Integration of a ring-shaped SMB in a ring-spinning tester *IEEE Trans. Appl. Supercond.* **26** 3601105
[15] Hossain M *et al* 2017 Mathematical modeling, simulation and validation of the dynamic yarn path in a superconducting magnet bearing (SMB) ring spinning system *Text. Res. J.* **87** 1011–22
[16] Hossain M *et al* 2020 *In situ* measurement of dynamic yarn path in a turbo ring spinning process based on superconducting magnetic bearing twisting system *Text. Res. J.* **90** 951–68
[17] Sparing M *et al* 2016 Dynamics of rotating superconducting magnetic bearings in ring spinning *IEEE Trans. Appl. Supercond.* **26** 3600804
[18] Miyazaki Y *et al* 2016 Development of superconducting magnetic bearing for flywheel energy storage system *Cryogenics* **80** 234–7
[19] Yu Z *et al* 2019 Electromagnetic and rotational characteristics of a superconducting flywheel energy storage system utilizing a radial-type high-temperature superconducting bearing *J. Supercond. Novel Magn.* **32** 1605–16
[20] Cansiz A *et al* 2003 An evershed type superconducting flywheel bearing *Phys.* C **390** 305–10
[21] Sotelo C G *et al* 2016 Tests with a hybrid bearing for a flywheel energy storage system *Supercond. Sci. Technol.* **29** 095016
[22] Fukuyama H *et al* 1995 Static and dynamic characteristics of superconducting magnetic bearings using MPMG Y-Ba-Cu-O *JSME Inter. J.* C **38** 128–34
[23] Strasik M *et al* 2007 Design, fabrication, and test of a 5 kWh/100 kW flywheel energy storage utilizing a high-temperature superconducting bearing *IEEE Trans. Appl. Supercond.* **17** 2133–7
[24] Espenhahn T *et al* 2020 Influence of the magnet aspect ratio on the dynamic stiffness of a rotating superconducting magnetic bearing *J. Phys. D: Appl. Phys.* **53** 035002